Design of a Beam Separator for FLASH Electron Therapy Facilities

Vera Korchevnyuk, Jérémie Bauche, Mikko Karppinen, Andrea Latina, Stephan Russenschuck, Mike Seidel, and Davide Tommasini

***Abstract*—A promising modality of radiation therapy is FLASH: a technique in which the full radiation dose is delivered in just 1/10th of a second. This modality has been proven successful in destroying cancerous cells while sparing healthy tissues. The aim is to develop an accelerator to treat large-volume and deep-seated tumors using high-energy electron beams in the FLASH modality. Specifically, we are designing a steady-state magnet that guides three distinct energy beams into three separate beamlines and ensures dose conformality within FLASH timescales. This paper presents a design method that incorporates beam optics and magnetic parameters into a numerical optimization process. The method is applied to the design of a magnetic spectrometer with a varying pole profile. The magnet performance is compared to pure dipole and combined dipole-quadrupole designs.**

***Index Terms*—FLASH, accelerator magnets, magnet design, beam dynamics, spectrometer, optimization.**

I. Introduction

IN THE context of radiation therapy, an emerging and promising topic is the so-called FLASH therapy. It consists of delivering the entire radiation treatment in a few hundred milliseconds, whereas in conventional radiation therapy, the dose is delivered in minutes. This fast delivery of the dose has shown to successfully minimize damage to the surrounding healthy tissues, yet effectively destroying the tumor [1], [2]. A project to build the first clinical facility for treating deep-seated and large-volume tumors with FLASH high-energy electron beams has been approved [3], [4], [5]. A key element of this facility is the *beam separator*. The purpose of the beam separator is to guide pulsed beams coming from a linear accelerator into distinct beamlines. The beams follow different trajectories and meet again at the patient, from different directions, within FLASH timescales. Several conventional solutions for a beam separator were studied and proven insufficient for a compact facility. A varying pole profile along the longitudinal direction is the most suitable candidate geometry for the magnet. In the following sections, we present a design method based on particle tracking and expose the design case of the beam separator for the FLASH electron therapy facility.

Manuscript received 21 September 2023; revised 17 November 2023; accepted 22 November 2023. Date of publication 19 December 2023; date of current version 20 December 2023. This work was supported by the Knowledge Transfer at CERN. *(Corresponding author: V. Korchevnyuk.)*

Vera Korchevnyuk is with the École Polytechnique Fédérale de Lausanne (EPFL), 1015 Lausanne, Switzerland European Organization for Nuclear Research (CERN), 1211 Geneva, Switzerland (e-mail: vera.korchevnyuk@epfl.ch).

Jérémie Bauche, Mikko Karppinen, Andrea Latina, Stephan Russenschuck, and Davide Tommasini are with the European Organization for Nuclear Research (CERN), 1211 Geneva, Switzerland.

Mike Seidel is with the École Polytechnique Fédérale de Lausanne (EPFL), 1015 Lausanne, Switzerland.

Color versions of one or more figures in this article are available at https://doi.org/10.1109/TASC.2023.3341895.

Digital Object Identifier 10.1109/TASC.2023.3341895

II. The Design Method

The design of the beam separator, based on the tracking of particle beams, includes the following steps:

- Defining the design objectives for the magnet.
- Segmenting the magnet and retrieving the magnetic field multipoles that produce the desired solution for the output beams.
- Using these multipoles to describe the shape of the ideal iron pole profiles.
- Checking the consequences of truncating and revolving the iron pole.
- Simulating the magnet in 3D, extracting the field map, and evaluating the performance of the beam separator.

A. Setting Design Goals

We begin by establishing the design objectives for the magnet. These include separating the input beams along the magnet, adjusting their size, focus, or a combination of these. The goal of the present device is to maximize the separation between the three output beams while keeping their size and divergence as small as possible. Increasing the separation angle of the beam separator promotes compactness by reducing the requirement for extended drifts following the device, allowing for more immediate placement of additional optic elements. An additional goal of the design is to bend the middle-energy beam by 90 degrees.

B. Retrieving Optimal Magnet Parameters

The next step is determining the most suitable magnet parameters aligning with the desired objectives. For that, we treat the magnet as an ideal element that transforms the input beams into output beams. The element is divided into sectors and each of them is characterized by a set of magnetic multipoles. The size and strength of each of the magnetic multipoles are the *design variables* of the optimization problem. The design

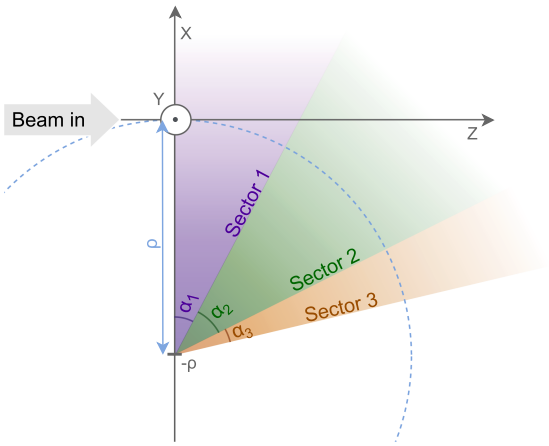

Fig. 1. Illustration of the field map. The domain is divided into sectors of angle α and characterized by a set of magnetic multipoles. Outside the sectors, $\vec{B} = 0$. The input beam enters the device along the z-axis.

variables are

$$\mathbf{X} = \begin{bmatrix} \alpha_1 & M_{11} & M_{12} & \dots & M_{1Q} \\ \alpha_2 & M_{21} & M_{22} & \dots & M_{2Q} \\ \vdots & \vdots & \vdots & \ddots & \vdots \\ \alpha_P & M_{P1} & M_{P2} & \dots & M_{PQ} \end{bmatrix}, \tag{1}$$

where P is the number of sectors in the defined setup and Q is the number of magnetic multipoles used to describe the field map[1]. Fig. 1 shows the described setup.

The variables in $\mathbf{X}$ are used to generate a magnetic-field model through which the particle beams are tracked. These beams are defined by their transverse and longitudinal coordinates x, y, z, transverse and longitudinal momenta p_x, p_y, p_z, mass m, and charge q. From these data, meaningful properties can be computed, such as horizontal and vertical size $b_{\mathrm{x}}(s)$ and $b_{\mathrm{y}}(s)$, horizontal and vertical divergence $d_{\mathrm{x}}(s)$ and $d_{\mathrm{y}}(s)$, energy spread of the beam δ, and separation angle between beams a. These properties are useful to evaluate the quality of the proposed solution and therefore steer the optimization.

We used the tracking code RF-Track [6] to simulate the beam trajectories and properties in the field model. This code propagates the particles by integrating the equations of motion using symplectic algorithms. It enables particle tracking in field maps, providing different interpolation methods, including linear, cubic, and divergence-free. As the code is fully integrated into programmable scientific codes such as Octave or Python, iterative optimization of the field directly based on the beam performance from tracking is possible.

To evaluate the quality of a solution, the weighted objective function

$$f = \min_{\mathbf{X}} \left\{ -q_1 a + q_2 \overline{b_{\mathrm{x}}} + q_3 \overline{b_{\mathrm{y}}} + q_4 \overline{d_{\mathrm{x}}} + q_5 \overline{d_{\mathrm{y}}} \right\} \tag{2}$$

is employed. In (2), q_i represent the weights of the different objectives, a corresponds to the separation angle between outer beams at the exit of the separator magnet, and $\overline{b_{\mathrm{x}}}$, $\overline{b_{\mathrm{y}}}$, $\overline{d_{\mathrm{x}}}$ and $\overline{d_{\mathrm{y}}}$ correspond to the average values for the horizontal size, vertical size, horizontal divergence and vertical divergence of the output beams, respectively.

As a starting point, the number of sectors and multipoles in the field model is $P = 2$ and $Q = 2$, however these numbers can be increased to improve the obtained solution. To guarantee the bending of the middle-energy beam by 90 degrees, $\|\vec{B}\|$ is kept constant along the reference trajectory, shown as a dashed line in Fig. 1. By making the radius of the central trajectory the same as the bending radius ρ and the sum of all angles α equal to 90 degrees, the beam is transformed as intended.

After running the optimization routine, the optimal magnet parameters, as defined in (1), are

$$\mathbf{X}_{\mathrm{opt}} = \begin{bmatrix} 35\,\mathrm{deg.} & -0.57\,\mathrm{T} & -0.7\,\mathrm{T/m} \\ 55\,\mathrm{deg.} & -0.57\,\mathrm{T} & 2.4\,\mathrm{T/m} \end{bmatrix}. \tag{3}$$

The simplex optimization algorithm is described in [7].

C. Computing the Ideal Pole Profile

Once the optimal multipoles per sector are obtained, we move on to designing the cross-section of each sector.

Expressing the magnetic scalar potential as

$$\phi_{\mathrm{m}}(x, y) = \mathrm{Im}\left\{ \sum_{n=1}^{\infty} -\frac{B_n + iA_n}{nR_{\mathrm{ref}}^{n-1}} (x + iy)^n \right\}, \tag{4}$$

the ideal pole profile corresponds to the equipotential lines. To obtain the equipotential lines, it is enough to set ϕ_{m} to a constant [8], [9].

In the case of a combined dipole-quadrupole magnet with multipole order $n = \{1, 2\}$ and perfect up-down symmetry, there are only B_1 and B_2. As described in [10], this results in the family of curves

$$y(x) = \frac{K}{M_1 + M_2 x} \tag{5}$$

where K is a constant proportional to the magnetomotive force of the element (measured in ampere-turns). These curves are hyperbolas, with asymptotes at $x = -\frac{M_1}{M_2}$ and $y = 0$.

Given that the present design only has two sectors, $N = 2$, the two equations for the pole profile – one per sector – are

$$y_1(x) = \frac{-0.0113}{-0.57 - 0.7x} \tag{6}$$

$$y_2(x) = \frac{-0.0113}{-0.57 + 2.4x}, \tag{7}$$

both in m. Fig. 2 shows the shape of the ideal pole profiles for the two sectors.

D. Truncating and Revolving the Pole Profile

The pole profile equation defined with the scalar potential method requires infinitely wide poles and assumes a straight magnet. As this is not the case for the required beam separator,

[1]The magnetic multipoles M_n are related to the magnetic harmonics B_n by $M_n = B_n \frac{(n-1)!}{R_{\mathrm{ref}}^{n-1}}$.

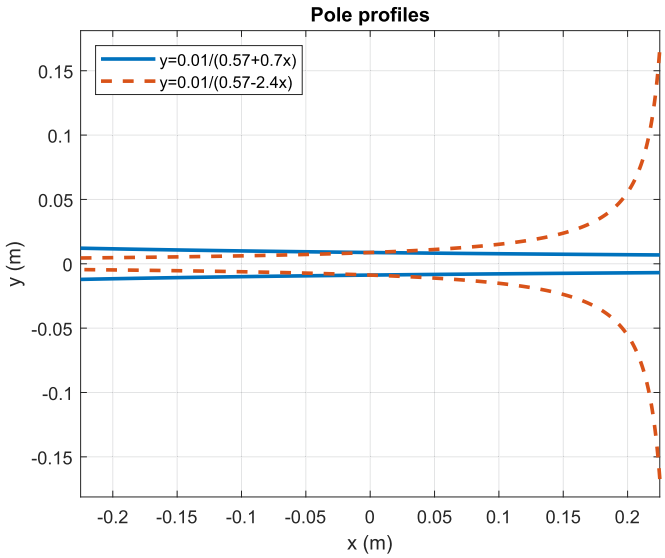

Fig. 2. Illustration of the iron pole profiles for different multipoles and K values.

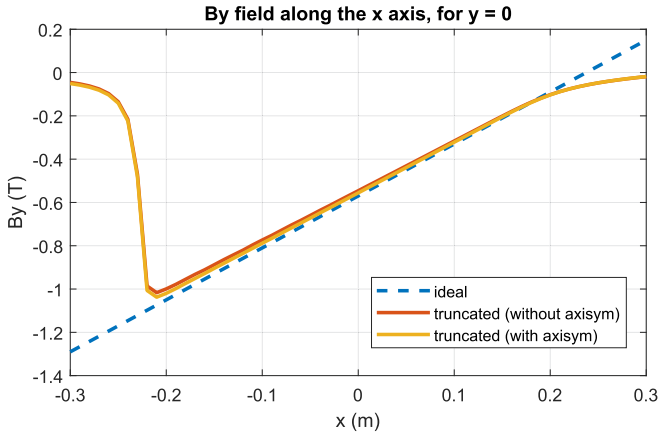

Fig. 3. Magnetic field along the x-axis of a truncated and an ideal pole profile. The pole was truncated at $x = \pm 225$ mm.

the consequences of truncating and revolving the resulting pole profile must be evaluated.

The size of the gap between the poles remains within defined limits, $2y_{\text{min}}$ and $2y_{\text{max}}$. For a dipole-quadrupole combined function to remain within the defined aperture sizes, the pole has to be truncated at x_{a} and x_{b} related by

$$x_{\text{a}} = \left(\frac{y_{\text{min}}}{y_{\text{max}}} - 1\right)\frac{M_1}{M_2} + \frac{y_{\text{min}}}{y_{\text{max}}}x_{\text{b}}. \tag{8}$$

To keep the central beam at $x = 0$ at the entrance of the separator, it follows that $x_{\text{a}} = -x_{\text{b}}$, and therefore

$$x_{\text{a}} = \frac{M_1}{M_2}\left(\frac{y_{\text{min}} - y_{\text{max}}}{y_{\text{min}} + y_{\text{max}}}\right). \tag{9}$$

To facilitate the manufacturing and measurement processes, the gap size is kept between 10 and 400 mm. Using (9), the truncation for each sector is

$$x_{\text{a1}} = -x_{\text{b1}} = 0.775\,\text{m} \tag{10}$$

$$x_{\text{a2}} = -x_{\text{b2}} = 0.226\,\text{m}. \tag{11}$$

Taking the smallest value of the two and allowing a small margin, the pole of the magnet extends from $x = -225$ mm to $x = 225$ mm. Using these geometrical parameters a 2D magnetic field simulation is carried out, using the coupling method of boundary and finite elements implemented in the CERN field computation program ROXIE [11]. The ampere-turns, NI, depend on the B_1 and the size of the gap, y_{c}, between the poles in the center of the magnet, i.e., at $x = 0$.

$$NI = \frac{2\,y_{\text{c}}M_1}{\mu_0}, \tag{12}$$

where μ_0 is the magnetic permeability. In the present design, $NI = 8992.3$ A. Fig. 3 shows the consequence of truncating the ideal pole profile: it shows B_y along the x-axis at $y = 0$ for both the ideal and truncated pole profiles (both without and with axisymmetry). From $x = -200$ mm to $x = 200$ mm, the difference between the magnetic field generated by the ideal pole and the truncated pole is below 0.05 T.

TABLE I
MULTIPOLES GENERATED WITHOUT AND WITH AXISYMMETRY

	Without axisymmetry	With axisymmetry
M_1, in T	-0.5458	-0.5557
M_2, in T/m	2.2887	2.3329
M_3, in T/m^2	0.1710	0.1234
M_4, in T/m^3	1.0327	1.7436
M_5, in T/m^4	-19.4152	-3.1634

The pole profile obtained from (4) describes the pole of a straight magnet. However, a *sector-bend*, as shown in Fig. 1, with a radius of curvature $\rho = 0.7$ m is required. The revolution will affect the magnetic length of the various beams. Moreover, the difference in the surface of the pole and return leg introduces unwanted higher-order harmonics. This is studied by computing an axisymmetric field model in ROXIE. This can easily be accomplished because the boundary-element method does not require the meshing of the air domain and the far-field boundary conditions.

For sector 2, the ideal pole profile is described by (7). Fig. 4 shows the $\|\vec{B}\|$ in the iron with and without axisymmetry and Table I gives the multipoles generated in both cases. Even at this relatively small bending radius, the effect of the revolution on the air-gap flux density remains below 2 % and for the higher-order harmonics below 5 %.

E. Building the 3D Magnetic Model

To understand the effects that the transitions between the sectors, the fringe fields, and the pole-face rotation have on the beams, a 3D magnetic model was built, using Dassault-OPERA3D [12]. Figure 5 shows the resulting 3D model of the beam separator (CAD and FE model). The transition area between the two sectors is morphed and the exit of the magnet is trimmed to bring the pole face rotation to zero.

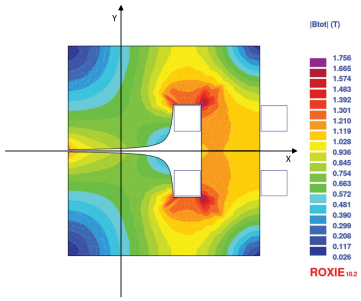

(a) Without axisymmetry.

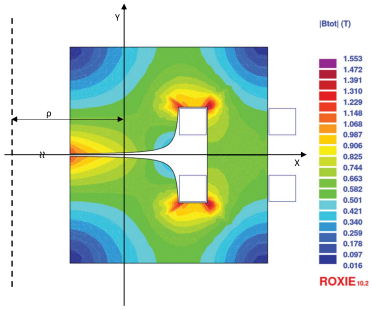

(b) With axisymmetry (axis at $x = -\rho$).

Fig. 4. Magnetic simulation in 2D of the pole profile defined by $K = -0.0113$, $M_1 = -0.57$ T and $M_2 = 2.4$ T/m.

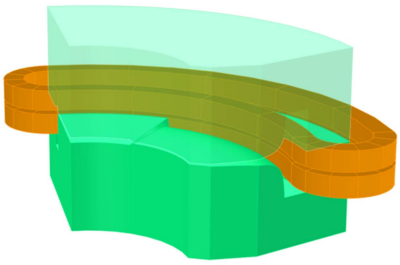

(a) CAD model of the beam separator.

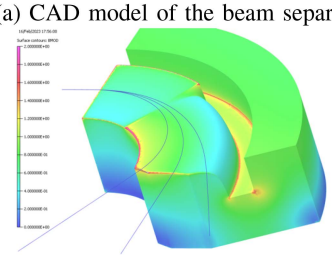

(b) Magnetic simulation in 3D.

Fig. 5. 3D model of the beam separator with two combined-function sectors.

F. Evaluating the Performance of the Design

Finally, the field map generated by the 3D magnetic model is exported and used as input in the particle tracking software. The input beam is a homogeneous beam of 1000 particles, with horizontal radius of 1 mm, vertical radius of 1.5 mm, horizontal divergence of 1.5 mrad, vertical divergence of 1 mrad, and energy spread of 0.5 %. The result of the tracking is shown

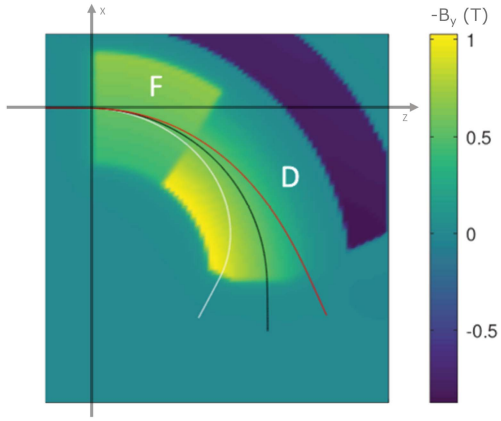

Fig. 6. Particle tracking of three beams through the magnetic field generated by the 3D model of the 2-sector separator magnet.

TABLE II
OUTPUT BEAM PARAMETERS FOR THREE POSSIBLE SOLUTIONS FOR THE BEAM SEPARATOR: A PURE DIPOLE, A 1-SECTOR COMBINED FUNCTION (DIPOLE+QUADRUPOLE) AND A 2-SECTOR COMBINED FUNCTION (DIPOLE+QUADRUPOLE). P, α, B_X, B_Y, D_X, D_Y ARE THE BEAM MOMENTUM, EXIT ANGLE, HALF HORIZONTAL BEAM SIZE, HALF VERTICAL BEAM SIZE, HALF HORIZONTAL BEAM DIVERGENCE AND HALF VERTICAL BEAM DIVERGENCE. THESE PARAMETERS WERE GENERATED BY TRACKING THE INPUT BEAM THROUGH MAGNETIC FIELD MAPS

	P (MeV/c)	α **(deg.)**	$\mathbf{b_x}$ **(mm)**	$\mathbf{b_y}$**, (mm)**	$\mathbf{d_x}$ **(mrad)**	$\mathbf{d_y}$ **(mrad)**
1 Sect. (Dip.)	100	102.04	5.00	3.58	7.03	2.54
	120	90.41	5.06	3.83	5.74	2.52
	140	82.14	5.61	3.93	5.11	2.44
1 Sect. (Dip.+ Quad.)	100	119.44	4.59	4.85	15.70	2.54
	120	88.88	22.40	4.39	33.28	2.68
	140	62.07	22.75	4.45	35.24	2.54
2 Sect.: (Dip.+ Quad.)	100	118.31	8.92	4.79	12.36	2.52
	120	89.73	12.68	4.75	19.37	2.54
	140	65.78	13.84	4.67	21.44	2.54

in Fig. 6 and the output beam properties are given in Table II. From the exit angles, the separation angle is $a = 52.5$ degrees. For comparison, the separation angle provided by the pure dipole solution is $a \approx 20$ degrees. For the 1-sector combined function dipole-quadrupole solution, one can achieve $a = 57.38$ degrees, however, the horizontal size and divergence of the output beams is approximately $40\,\%$ higher than for the new 2-sector solution.

III. DISCUSSION

The current design fulfills the project's requirements and yields an improved solution compared to the pure-dipole or 1-sector dipole-quadrupole solutions. Choosing a 2-sector design as opposed to more was a compromise between the complexity of the design and the effect on the beam. There is also a compromise in terms of separation angle and the size and divergence of the output beams: increasing one and decreasing the other are two counteracting effects. For the manufacturing of the device, we do not expect major challenges. The yoke can be machined from a block of solid iron, and the copper coils can be produced by conventional winding. The design of the field transducer for the magnetic measurement of this curved magnet shall be investigated. Some options are: probing the aperture

with a Hall sensor to reconstruct the field map and using a curved coil magnetometer for the integrated bending strength. Ideally, beam-based measurements would be performed.

IV. Conclusion

The proposed method for designing the beam separator offers a compact solution well-suited for implementation in a FLASH medical facility. Other projects with demanding beam requirements can benefit from this beam-based magnet design. The device is designed for steady-state operation, enabling high repetition rate beams. Its complexity resides in its design rather than its operation. Compared to pure dipole and 1-sector combined dipole-quadrupole solutions, the new 2-sector design offers a better balance between the separation angle and the horizontal beam size and divergence.

References

[1] M. C. Vozenin, J. H. Hendry, and C. L. Limoli, "Biological benefits of ultra-high dose rate FLASH radiotherapy: Sleeping beauty awoken," *Clin. Oncol.*, vol. 31, no. 7, pp. 407–415, 2019.

[2] J. Bourhis et al., "Treatment of a first patient with FLASH-radiotherapy," *Radiotherapy Oncol.*, vol. 139, pp. 18–22, 2019.

[3] M. Dosanjh, R. Corsini, A. Faus-Golfe, and M.-C. Vozenin, "Very high-energy electrons for cancer therapy," *CERN Courier*, 2020. [Online]. Available: https://cerncourier.com/a/very-high-energy-electrons-for-cancer-therapy/

[4] W. Wuensch, "An accelerator system for the FLASH treatment of large deep-seated tumors," in *Academic Training Lecture Regular Programme. CERN*, 2022. [Online]. Available: https://indico.cern.ch/event/1131207/

[5] "FLASH: An innovative electron radiotherapy technology," [Online]. Available: https://kt.cern/flash-radiotherapy

[6] A. Latina, "RF-Track reference manual," 2020. [Online]. Available: https://zenodo.org/record/4580369

[7] J. C. Lagarias, J. A. Reeds, M. H. Wright, and P. E. Wright, "Convergence properties of the Nelder–Mead simplex method in low dimensions," *SIAM J. Optim.*, vol. 9, no. 1, pp. 112–147, 1998.

[8] S. Russenschuck, *Field Computation for Accelerator Magnets: Analytical and Numerical Methods for Electromagnetic Design and Optimization*. Hoboken, NJ, USA: Wiley, 2010.

[9] J. T. Tanabe, *Iron Dominated Electromagnets: Design, Fabrication, Assembly and Measurements*. Singapore: World Sci., 2005.

[10] A. Milanese, "Tracking magnetic equipotential curves for general combinations of multipolar fields," 2022. [Online]. Available: https://edms.cern.ch/document/2792136/1

[11] S. Russenschuck, "ROXIE," [Online]. Available: https://roxie.docs.cern.ch/

[12] "SIMULIA Opera 3D," 2021. [Online]. Available: https://www.3ds.com/products-services/simulia/products/opera/